

NONLINEAR ANALYSIS OF JUXTACRINE PATTERNS*

HELEN J. WEARING[†] AND JONATHAN A. SHERRATT[†]

Abstract. We investigate a discrete mathematical model for a type of cell-cell communication in early development which has the potential to generate a wide range of spatial patterns. Our previous work on this model has highlighted surprising differences between the predictions of linear analysis and the results of numerical simulations. In particular, there is no quantitative agreement between the unstable modes derived from linear analysis and the patterns observed numerically. In this paper, we look at the nonlinear model on a domain of two cells with the aim of gaining an insight into behavior in larger systems. We study the existence and stability of spatially heterogeneous steady-state solutions, which correspond to patterns of alternating cell fate on larger domains, as we vary two key parameters. These parameters are measures of the strength of positive feedback in the biological system. By reducing the problem to two coupled nonlinear algebraic equations, we show that a patterned solution exists and is stable on a 2-cell domain for a significant part of parameter space. We compare these results to those obtained from linear analysis and conclude that the behavior of the nonlinear 2-cell system gives a better insight into the results of numerical simulations on large arrays of cells. Furthermore, we conduct a bifurcation analysis of the model on domains of various sizes: we demonstrate that as the domain size increases, the 2-cell pattern becomes unstable for certain parameters, and overall the number of stable patterns increases. This leads us to speculate that on large domains there are many stable patterned solutions to the model of approximately the same periodicity, which is typical of the fine-grained patterns that one sees during early development. Our work predicts that this is a feature of the patterning dynamics rather than a consequence of environmental heterogeneity.

Key words. pattern formation, juxtacrine signaling, positive feedback, bifurcation analysis

AMS subject classifications. 92C15, 92C37, 34C23

PII. S003613990037220X

1. Introduction. Early development in organisms is characterized by the determination of cell fate—for example, whether a cell will become part of a bone or part of the surrounding soft tissue. In general, this occurs on a very small spatial scale, whereby a single cell adopts a different fate from that of its neighbors. This microscopic pattern formation is common in the early stages of neural development [9]. It is thought that direct communication between neighboring cells is one way in which these patterns are generated. Such a mechanism is of particular interest in epithelial tissues, in which cells are closely packed together with little intercellular space.

The basis of cellular communication is that a molecule of a signaling chemical, known generically as a ligand, binds to a receptor on the cell surface. This can regulate many properties of a cell, such as, its growth rate or adhesiveness. Moreover, the receptor complex can also regulate the production of new ligand and receptor molecules within the cell. Traditionally, cell signaling pathways were divided into three categories: autocrine—the molecule acts on the cell that produces it; paracrine—

*Received by the editors May 17, 2000; accepted for publication (in revised form) April 2, 2001; published electronically August 22, 2001. The research of the first author was supported by a research studentship from the Biotechnology and Biological Sciences Research Council. The research of the second author was supported by an advanced research fellowship from the Engineering and Physical Sciences Research Council. The Centre for Theoretical Modelling in Medicine is supported by a Research Development Grant from the Scottish Higher Education Funding Council.

<http://www.siam.org/journals/siap/62-1/37220.html>

[†]Centre for Theoretical Modelling in Medicine, Department of Mathematics, Heriot-Watt University, Edinburgh EH14 4AS, UK (helenw@ma.hw.ac.uk, jas@ma.hw.ac.uk).

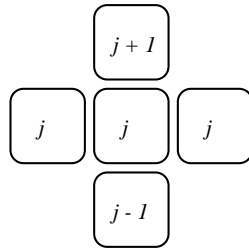


FIG. 1. We solve our model on a two-dimensional cellular array in which each cell in row j is identical, so that behavior varies only in one direction. Pattern formation thus corresponds to the generation of stripes within a two-dimensional sheet.

the molecule acts on neighboring cells via extracellular diffusion; and endocrine—the molecule acts on all cells within a tissue. However, in the 1980's a fourth mechanism was identified [11]: juxtacrine—where the signaling molecule is anchored in the surface of a cell and acts on immediately neighboring cells. This is possible only in tissues where the cells are in close contact with one another, most notably the epithelia that cover the surface of all tissues in the body. It is in these epithelia that much early developmental patterning occurs.

Several ligand-receptor systems that operate via juxtacrine signaling have been identified in developmental biology. In particular, there is a protein called Delta which binds to the receptor Notch [13, 10]; this interaction is known to be important in early development of the fruitfly. A previous mathematical model by Collier et al. [6] looked at the Delta-Notch mechanism under the assumption that receptor activation downregulated ligand production. Their work showed that given sufficiently strong feedback, the model was capable of generating fine-grained patterns, in which cells alternate between high and low levels of Delta and Notch expression. Patterns of wavelength two cells are indeed observed in early development, but there are also many microscopic patterns of a somewhat longer wavelength, which are not predicted by Collier et al.'s mechanism. A possible resolution of this is that in some juxtacrine signaling mechanisms, receptor activation upregulates ligand production—the reverse of Collier et al.'s assumption. In fact, such upregulation is well established for certain juxtacrine signals [18], in particular, the binding of the ligands transforming growth factor- α and epidermal growth factor to the epidermal growth factor receptor [4, 5]. Moreover, recent experiments show that the important Delta-Notch system can exhibit this positive feedback in some contexts [1, 8, 10, 16]. Our work is concerned with the exploration of the patterning potential of juxtacrine signaling when this positive feedback occurs.

The specific mathematical model we consider was developed in [14] and, in accordance with the scale of the process, uses a discrete formulation, with ODEs representing ligand and receptor levels on each cell in a fixed cellular array. At the stage when early developmental patterns are being laid down, most epithelia are simply two-dimensional sheets of cells; later in development, these will thicken to be several cells deep. We restrict our attention to the formation of striped patterns within this sheet, although the same mechanism can give spotted and other two-dimensional patterns. Thus our model assumes a number of rows of cells with the model variables being the number of ligand molecules a_j , free receptors f_j , and bound receptors b_j , on the surface of cells in row j . A sketch of the cellular array that we use is given in Figure 1.

The model equations are given by

$$(1a) \quad \frac{\partial a_j}{\partial t} = - \overbrace{k_a a_j \langle f_j \rangle}^{\text{binding}} + \overbrace{k_d \langle b_j \rangle}^{\text{dissociation}} - \overbrace{d_a a_j}^{\text{decay}} + \overbrace{P_a(b_j)}^{\text{production}},$$

$$(1b) \quad \frac{\partial f_j}{\partial t} = -k_a \langle a_j \rangle f_j + k_d b_j - d_f f_j + P_f(b_j),$$

$$(1c) \quad \frac{\partial b_j}{\partial t} = +k_a \langle a_j \rangle f_j - k_d b_j - \overbrace{k_i b_j}^{\text{internalization}},$$

where d_a, d_f, k_a, k_d, k_i are all positive constants. The kinetic scheme we use is as generic as possible: ligand and receptor molecules bind reversibly to form a bound receptor complex which can be internalized within the cell. We base rates of reaction on the law of mass action, and we assume that both ligand and free receptors decay at a constant rate. We assume that the production terms of new ligands and receptors, P_a and P_f , are increasing, saturating functions of the number of bound receptors. Particular forms will be discussed later, but note that we take $P_f(0)$ to be nonzero, reflecting the background production of free receptors in the absence of binding. The spatial coupling between the cells, $\langle \cdot \rangle$, is our representation of the juxtacrine communication. In this model, we assume that each cell has four nearest neighbors—two in the same row and one in each of the two adjacent rows. Under these assumptions the local average is then

$$(2) \quad \langle a_j \rangle \equiv \frac{a_{j-1} + 2a_j + a_{j+1}}{4}, \text{ etc.}$$

Of course, the cells in real epithelia are not arranged in regular geometric arrays, but our assumption enables detailed analysis of the process, which would otherwise be restricted to numerical simulation.

2. Previous work. The pattern-forming potential of the “one-dimensional” model, as described in section 1, was studied using local stability analysis in [21] and was supported by numerical simulations on large arrays of cells. In contrast to the mechanism studied by Collier et al. [6], we demonstrated that our juxtacrine model (1) can generate a wide range of pattern wavelengths. This result is clear from both the analysis of the linearized model and the numerical simulations of the full nonlinear model. Indeed, the linear analysis gives a fair insight into the behavior we observe in numerical simulations. However, it is evident that the nonlinearities override some of the predictions made by the linear analysis, and this is what we aim to address in the present work. Before we do this, it is helpful to present a summary of the previous results.

In the linear analysis, we applied techniques similar to those used by Turing [19] to investigate diffusion-driven instability in reaction-diffusion systems. This involves studying the stability of a uniform equilibrium subject to spatial perturbations. By varying certain parameters, we consider where this equilibrium is both stable to homogeneous perturbations and unstable to inhomogeneous perturbations, and we thus obtain a parameter regime where pattern formation is possible. Our parameter space is characterized by measures of the strength of ligand and receptor feedback at the uniform steady state. This is important since the nonlinear positive feedback in ligand and receptor production is the main assumption of our model. In addition, there

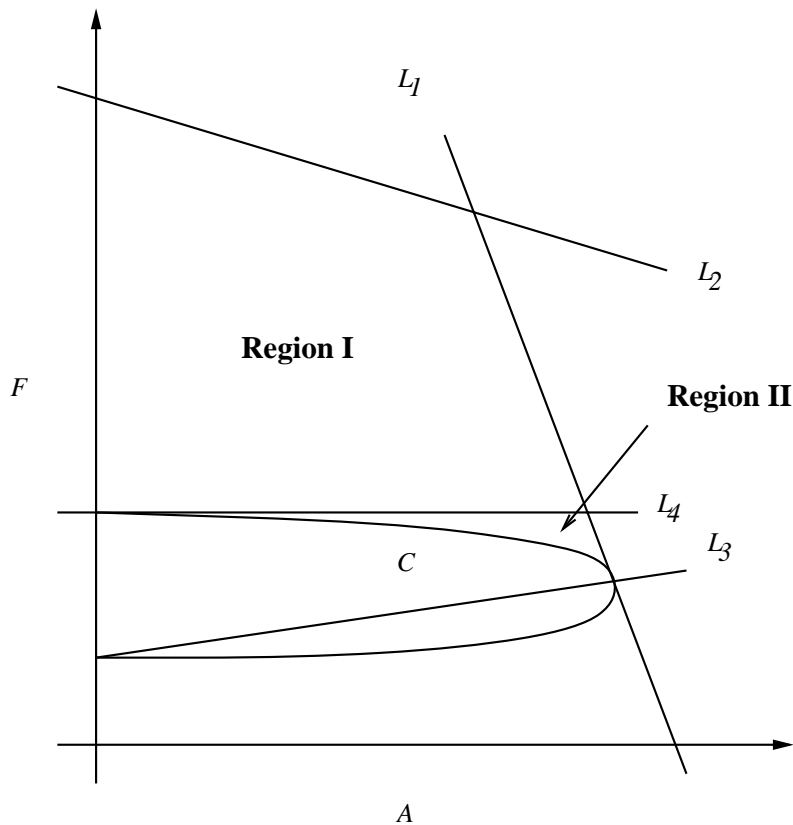


FIG. 2. Qualitative illustration of the parameter space in the $\mathcal{A} - \mathcal{F}$ plane, where pattern formation is possible. The parameters \mathcal{A} and \mathcal{F} represent, respectively, the slopes of the ligand and receptor feedback functions (P'_a and P'_f) at the homogeneous steady state. Below the lines \mathcal{L}_1 and \mathcal{L}_2 , the homogeneous equilibrium is stable to homogeneous perturbations. Above the curve C and the line \mathcal{L}_3 , the steady state is also unstable to inhomogeneous perturbations. The region for pattern formation is therefore defined by the \mathcal{F} -axis, the lines \mathcal{L}_1 and \mathcal{L}_2 , and the curve C . For mathematical convenience, we divide this region into two parts by the horizontal line \mathcal{L}_4 : below \mathcal{L}_4 , a wavelength of two cells is always a stable mode, whereas above \mathcal{L}_4 , a wavelength of two cells is always an unstable mode. Mathematical expressions for the lines $\mathcal{L}_1 - \mathcal{L}_4$ and the curve C are derived in [21].

exists empirical data for the kinetic rate constants of binding, dissociation, and internalization for specific signaling systems, but there is little data on feedback levels. Figure 2 illustrates the region of pattern formation in the $\mathcal{A} - \mathcal{F}$ plane, where \mathcal{A} and \mathcal{F} are, respectively, the slopes of the ligand and receptor feedback functions (P'_a and P'_f) at the homogeneous steady state. The lines that delimit this region were derived in [21] and will be referred to later in this work.

The linear analysis not only predicts when patterns will form but also the range of wavelengths that can destabilize the steady state for particular parameter values. Furthermore, we are able to estimate analytically and calculate numerically the wavelength that corresponds to the fastest growing mode, which is the wavelength we expect to dominate. Before discussing numerical simulations of the full nonlinear model, we therefore review the range of patterns that is predicted by the linear analysis. It turns out to be mathematically convenient to divide the region of pattern formation into two smaller regions (I and II), as shown in Figure 2. We use the term

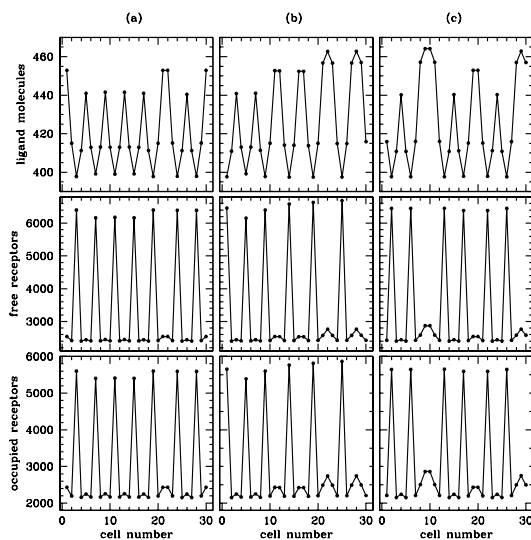


FIG. 3. Three numerical simulations of the model (1) on a domain of 30 cells, each corresponding to different (random) initial conditions. Linear analysis predicts the formation of a pattern with a wavelength of two cells. In all the simulations of the nonlinear equations for these parameter values we observe no regular form of pattern. The nearest solution to a pattern with a wavelength of four cells is illustrated in (a); a regular pattern of mode four is not possible in this case since 4 is not a divisor of 30. Notice that the high isolated peaks in the number of free and bound receptors are always at least four cells apart. Boundary conditions are periodic. The kinetic rate constants are $k_a = 0.0003 \text{ molecule}^{-1} \text{ min}^{-1}$, $k_d = 0.12 \text{ min}^{-1}$, $k_i = 0.019 \text{ min}^{-1}$, $d_a = 0.006 \text{ min}^{-1}$, $d_f = 0.03 \text{ min}^{-1}$. The feedback functions are taken to be of Hill form, such that $P_f = C_3 + (C_4^n b^n)/(C_5^n + b^n)$ and $P_a = (C_1^m b^m)/(C_2^m + b^m)$, where $C_1^m = 118$, $C_2 = 2500$, $C_3 = 90$, $C_4 = 6.9$, $C_5 = 5334$, $m = 0.1$, and $n = 3.02$. The profiles are for $t = 1800$ hours.

“single-mode pattern” to denote a pattern where only one wavelength is unstable; when there is a range of unstable wavelengths we shall refer to the pattern as “multimode.” Our analysis shows that single-mode patterns with a wavelength greater than two cell lengths are possible only in region II, and in theory there is no bound on the unstable wavelength in some parts of the parameter space. Multimode patterns are possible in both regions with no upper bound for the wavelength in either region; a pattern of wavelength two is always unstable in region I. The wavelength corresponding to the fastest growing mode takes the values 2 or 3 in region I, but it may take any value above 2 in region II.

The main goal of the numerical work in [21] was to test the predictions of our linear analysis and therefore add to our understanding of the nonlinear system. Numerical simulations were performed on arrays of 30 and 60 cells with periodic boundary conditions to simulate cells as part of a continuum. Initial conditions were random perturbations about the homogeneous steady state. Figure 3 shows three typical simulations for a single set of parameters. These solutions are characteristic of most of the simulations—a pattern that has some irregularities but with isolated peaks having a roughly constant separation. However, we also obtained patterns that were strictly periodic—for example, a peak in the number of bound receptors every five cells. In practice, only divisors of the number of cells in the array can be regular wavelengths; so for 30 cells these are 2, 3, 5, 6, 10, 15, and 30. By varying the feedback parameters, a wide range of different wavelength patterns was observed.

The motivation for this paper comes from the comparison of our numerical simulations with the predictions of the linear analysis. In short, the linear analysis seems to predict correctly the parameter regions in which patterns will form. Furthermore, as we vary the feedback parameters, numerical results agree qualitatively with the changes in the fastest growing mode. However, the wavelengths seen in the simulations do not agree quantitatively with the predictions of the linear analysis. In particular, for a large part of the parameter space, a wavelength of two cells, corresponding to an alternating pattern of high and low receptor numbers, is predicted to be the fastest growing mode by linear analysis. This is the case for the parameter values in Figure 3; indeed, a wavelength of two cells is the only unstable mode for these parameters. However, as demonstrated in Figure 3, a regular pattern of wavelength two is rarely observed in simulations on large arrays of cells.

The aim of the present work is to investigate the full nonlinear model for the 2-cell system and study the possibility of nonuniform steady states, which correspond to a pattern of alternating cell fates in larger systems. In section 3, we consider the steady-state equations of the model on an array of two cells; we show how these simplify to two coupled nonlinear equations and outline our approach to finding heterogeneous solutions. Section 4 analyzes these equations when the feedback functions are of a particular form and derives conditions for patterned equilibria; some of the mathematical details are rather laborious and are presented in the appendix. We then discuss these results in section 5 in the context of our previous work, investigating the stability of the 2-cell pattern in larger systems. Section 6 is left for a general discussion of the work.

3. Equilibria of the 2-cell system. Our analysis focuses on the model equations (1) for a 2-cell domain with periodic boundary conditions. In real systems, the juxtacrine mechanism will be functioning on much larger domains with tens, possibly hundreds, of cell numbers. However, the behavior of the 2-cell system may be a good indication as to what is occurring in larger arrays of cells and enables us to consider a reduced system of six coupled ODEs, for which the solutions are either homogeneous or patterned with a wavelength of two cells. In fact, for the striped patterns that we are considering (see Figure 1), the juxtacrine term is the same for both cells, i.e.,

$$(3) \quad \langle a_j \rangle = \frac{a_1 + a_2}{2}, \text{ etc. for } j = 1, 2,$$

and this simplifies the ODEs considerably. Indeed, when the system is at equilibrium, the end result is just two equations for the variables b_1 and b_2 .

Initially, the steady-state equation of (1c) yields

$$(4) \quad f_j = \frac{(k_d + k_i)b_j}{k_a \langle a_j \rangle} = \frac{2(k_d + k_i)b_j}{k_a(a_1 + a_2)}, \quad j = 1, 2.$$

Substituting this expression for f_j into (1a)–(1b), the equilibria of the 2-cell system are then determined by four nonlinear equations. These are given by

$$(5a) \quad 0 = -\frac{(k_d + k_i)a_j(b_1 + b_2)}{(a_1 + a_2)} + k_d \frac{(b_1 + b_2)}{2} - d_a a_j + P_a(b_j),$$

$$(5b) \quad 0 = -k_i b_j - \frac{2d_f(k_d + k_i)b_j}{k_a(a_1 + a_2)} + P_f(b_j)$$

for $j = 1, 2$. Notice that the pair of equations for each cell is symmetric, since the spatial coupling is identical for both cells. On rearranging (5b) for $j = 1$ and $j = 2$

to find $a_1 + a_2$, we obtain the following expression:

$$(6) \quad a_1 + a_2 = \frac{2d_f(k_d + k_i)b_1}{k_a(P_f(b_1) - k_i b_1)} = \frac{2d_f(k_d + k_i)b_2}{k_a(P_f(b_2) - k_i b_2)}.$$

The second equality governing b_1 and b_2 then simplifies to

$$(7) \quad \frac{b_1}{P_f(b_1)} = \frac{b_2}{P_f(b_2)}.$$

To find another relation between b_1 and b_2 , we first deduce an expression for a_j . We take the first equality of (6) and substitute this into (5a) to obtain

$$(8) \quad a_j = \frac{d_f b_1 [k_d(b_1 + b_2) + 2P_a(b_j)]}{2d_a d_f b_1 + k_a(b_1 + b_2)(P_f(b_1) - k_i b_1)}, \quad j = 1, 2.$$

Notice that the difference between a_1 and a_2 corresponds to the difference between $P_a(b_1)$ and $P_a(b_2)$. After summing (8) for $j = 1$ and $j = 2$, we have another expression for $a_1 + a_2$, which we can then equate with (6) to give

$$\frac{2d_f b_1 [k_d(b_1 + b_2) + P_a(b_1) + P_a(b_2)]}{2d_a d_f b_1 + k_a(b_1 + b_2)(P_f(b_1) - k_i b_1)} = \frac{2d_f(k_d + k_i)b_1}{k_a(P_f(b_1) - k_i b_1)}.$$

This equation simplifies so that either $b_1 = 0$, corresponding to the trivial uniform steady state, or

$$(9) \quad k_a(P_f(b_1) - k_i b_1)[P_a(b_1) + P_a(b_2) - k_i(b_1 + b_2)] - 2d_a d_f(k_d + k_i)b_1 = 0.$$

Solutions (b_1, b_2) of (7) and (9) therefore define the steady states of the 2-cell system. The homogeneous steady states are given by those solutions for which $b_1 = b_2$.

We are interested in when patterned solutions to the 2-cell system exist. Therefore, we would like to find conditions on the feedback functions, P_a and P_f , that determine when the coupled equations (7) and (9) have solutions such that $b_1 \neq b_2$. Our approach is motivated by the symmetry imposed by the juxtacrine average. Equation (7) is symmetric in b_1 and b_2 ; we thus use this equality to obtain another symmetric equation from (9) and study two symmetric equations instead. Each equation is considered individually; we will investigate for which parameters there are solutions satisfying $b_1 \neq b_2$ and visualize these solutions in the $b_1 - b_2$ plane. The intersections of the solution curves for each equation in the $b_1 - b_2$ plane correspond to the steady states of the system. We outline our investigation of these intersections for specific (biologically realistic) forms of the functions P_a and P_f in section 4. Further details of this analysis are presented in the appendix together with a simpler case for illustration.

We begin by considering (7), since this involves only one of the production functions, P_f . In particular, by defining $F(b) \equiv b/P_f(b)$ we are interested in solutions of $F(b_1) = F(b_2)$ for $b_1 \neq b_2$. We therefore require that F has at least one turning point. By direct differentiation, $F'(b) = 0$ if and only if

$$(10) \quad P_f(b) - bP'_f(b) = 0.$$

If (10) has no real and positive solution, then no patterned steady state can exist. Figure 4 illustrates the function $F(b)$ and solutions of $F(b_1) = F(b_2)$ in the $b_1 - b_2$ plane for a specific function P_f that satisfies (10) for some $b > 0$. The symmetry of (7)

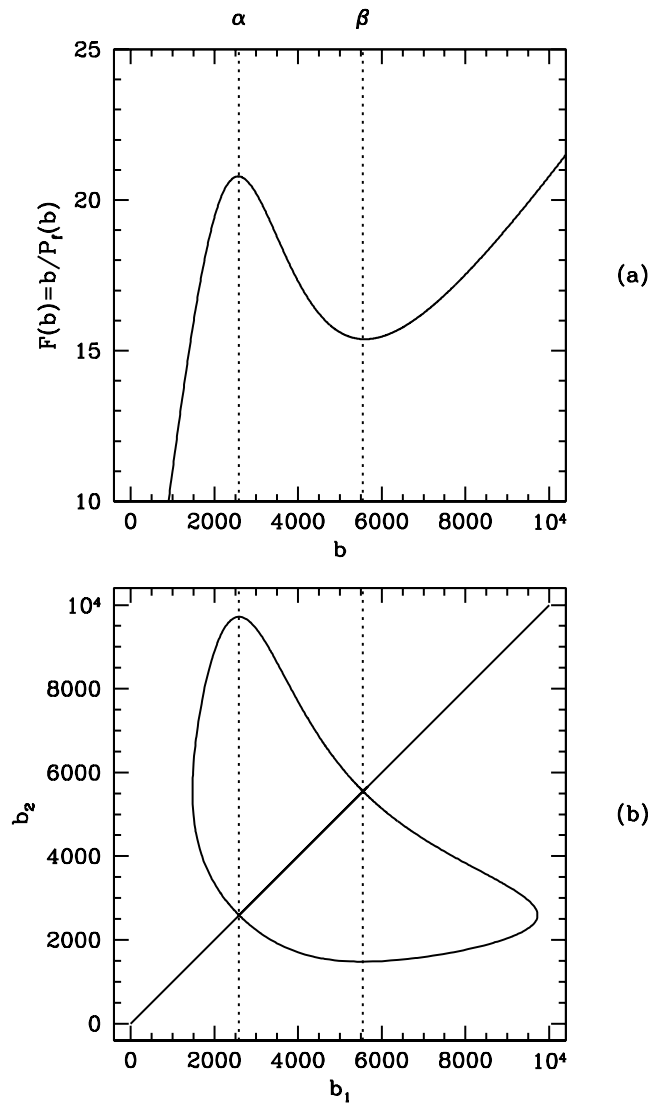


FIG. 4. Illustration of (a) $F = b/P_f(b)$ and (b) the solutions of $F(b_1) = F(b_2)$ for $P_f = C_3 + (C_4^n b^n)/(C_5^n + b^n)$, where $n = 4$, $C_3 = 90$, $C_4 = 4.5$, $C_5 = 4700$. The branching points of the nonuniform solutions of $F(b_1) = F(b_2)$ are the turning points of F , denoted by α and β . Expressions for these points are given in the appendix.

means that we have to consider only solutions for which $b_1 < b_2$ and then reflect these in the line $b_1 = b_2$. Notice that the turning points of F , denoted by α and β , give the branching points of the heterogeneous solutions in the $b_1 - b_2$ plane. Expressions for α and β and the condition for solutions $b_1 \neq b_2$ for this example can be found in the appendix.

We also wish to know when (9) has solutions such that $b_1 \neq b_2$ and where these overlap with solutions of (7) to give heterogeneous steady states. To facilitate the analysis, we can rewrite (9) in a symmetric form. First, if we divide throughout by

b_1 , then (9) becomes

$$G(b_1)[H(b_1) + H(b_2)] = 2c,$$

where $G(b) = P_f(b)/b - k_i$, $H(b) = P_a(b) - k_i b$, and $c = d_a d_f (k_d + k_i)/k_a$. Collecting the terms in b_1 on the left-hand side and those in b_2 on the right-hand side gives

$$H(b_1) - \frac{2c}{G(b_1)} = -H(b_2).$$

From the identity (7) it follows that $G(b_1) = G(b_2)$. We can therefore make the substitution $2/G(b_1) = [1/G(b_1) + 1/G(b_2)]$ to obtain the following symmetric equation in b_1 and b_2 :

$$(11) \quad \Phi(b_1) = -\Phi(b_2),$$

where

$$(12) \quad \Phi(b) = H(b) - \frac{c}{G(b)} \equiv P_a(b) - k_i b - \frac{d_a d_f (k_d + k_i) b}{k_a (P_f(b) - k_i b)}.$$

The roots of Φ determine the homogeneous steady states. We are now interested in solutions of $\Phi(b_1) = -\Phi(b_2)$, such that $b_1 \neq b_2$, and where these coincide with those of $F(b_1) = F(b_2)$. Figure 5 displays the function Φ and solutions of $\Phi(b_1) = -\Phi(b_2)$ for specific forms of P_a and P_f . Since Φ depends on both production functions, its form can vary much more than that of F . However, there are properties of Φ that can be deduced from the biological constraints of the system. In particular, we can assume that $G(b) > 0$ for all $b < r_{max}$, where r_{max} is the maximum number of receptors that can be expressed on a cell's surface, since only at the point of saturation must the rate of internalization ($k_i b$) be equal to the rate of free receptor production ($P_f(b)$). Therefore, $\Phi < 0$ for all b such that $H < 0$. It is also easy to show that the turning points of $1/G(b)$ are identical to those of $F(b)$. In the next section, we consider solutions to (7) and (11) and their intersections for biologically realistic forms of the production functions.

4. Conditions for patterned solutions when P_a and P_f are of Hill function form. In this section we look at a specific case when both production functions are increasing, saturating functions of b . We investigate this case for a particular system in which the parameter values are fixed, except for two free parameters that give an indication of the feedback strength in ligand and free receptor production. By partitioning the parameter space, we deduce conditions that are necessary for the existence of patterned solutions to the 2-cell system.

We suppose that both functions have Hill form; these are the forms used in [21] and are defined as follows:

$$(13) \quad P_a(b) = \frac{C_1^m b^m}{C_2^m + b^m},$$

$$(14) \quad P_f(b) = C_3 + \frac{C_4^n b^n}{C_5^n + b^n},$$

where C_1, \dots, C_5 are positive constants and m and n are real numbers greater than zero. The two function forms differ qualitatively at $b = 0$, since $P_a(0) = 0$ and $P_f(0) = C_3$; as mentioned in section 1, we are assuming a background level of free receptors in

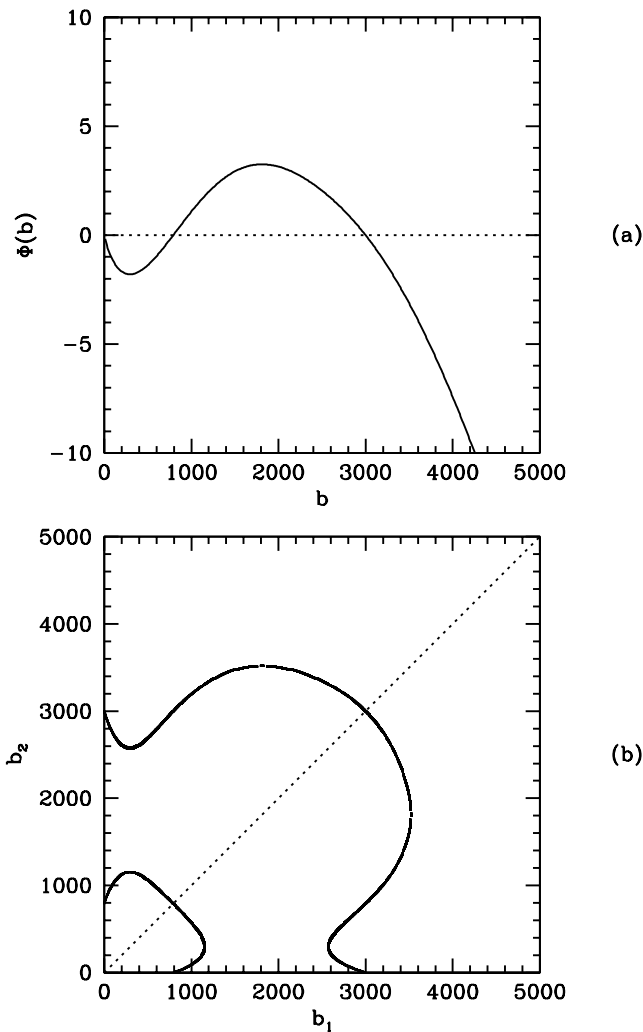


FIG. 5. (a) The form of $\Phi(b)$ and (b) the solutions of $\Phi(b_1) = -\Phi(b_2)$ in the $b_1 - b_2$ plane for $P_a = (C_1^m b^m)/(C_2^m + b^m)$ and P_f as in Figure 4, where $m = 1.5$, $n = 5$, $C_1 = 105$, $C_2 = 2500$, $C_3 = 90$, $C_4 = 3.3$, $C_5 = 4300$. Note that the roots of Φ are the points of intersection of the line $b_1 = b_2$ with $\Phi(b_1) = -\Phi(b_2)$.

the absence of binding so that P_f is nonzero at $b = 0$. We study Hill functions simply as a commonly used example of nonlinear feedback, and our calculations would apply for other similar functions; however, nonlinearity in $P_f(b)$ is essential for patterns to form.

If we fix one homogeneous steady state, say, (a_{eq}, f_{eq}, b_{eq}) , then this determines all but two of the parameters in the production functions in terms of the kinetic rate constants. The two “free” parameters (which are most conveniently taken as the Hill coefficients m and n) can be interpreted as a measure of the feedback strength and are equivalent to the parameters \mathcal{A} and \mathcal{F} in Figure 2 of our linear analysis. In this way we can study the behavior of the system in a two-dimensional parameter space, where we vary the strengths of the feedback in both ligand and free receptor production. For

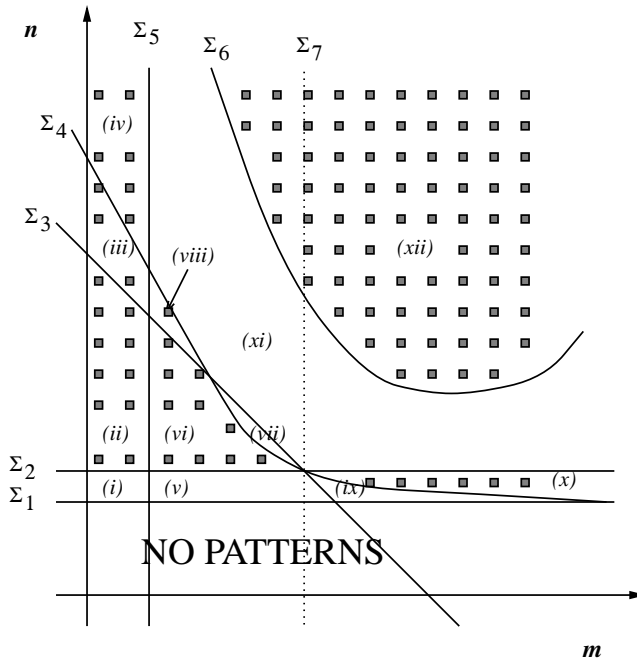


FIG. 6. Qualitative partition of the parameter space for the 2-cell system, where P_a and P_f are of Hill form. The parameters m and n (the Hill coefficients) represent the strength of ligand and receptor feedback, respectively. We delimit twelve regions by conditions on m and n , denoted by $\Sigma_1 - \Sigma_6$. (The dotted line Σ_7 denotes $H'(b_{eq}) = 0$ and is discussed in section A.2 of the appendix.) These regions are detailed in section A.2 of the appendix, although it is worth noting that values of n above the line Σ_1 satisfy the condition given by (A.2), which implies that heterogeneous solutions are not possible for the region below Σ_1 . Regions filled with grey squares are those where patterned solutions are possible. Patterned solutions are also possible for some parameters in region (xi). For comparison, the lines Σ_2 and Σ_3 correspond, respectively, to the lines \mathcal{L}_4 and \mathcal{L}_1 of Figure 2, which are derived in our linear analysis.

the other parameter values we use data on a specific juxtacrine mechanism, namely, the binding of the ligand transforming growth factor- α to the epidermal growth factor receptor. This data set was also used in [21] and will allow us to directly compare the nonlinear analysis presented in this work with the linear analysis and numerical simulations carried out in [21].

We partition the parameter space analytically by obtaining conditions on the feedback parameters m and n . The qualitative form of the partitioned parameter space is illustrated in Figure 6. These regions are constructed by considering the behavior of the functions $F(b)$ and $\Phi(b)$ as we increase the parameters m and n . This in turn affects the solution curves of (7) and (11) and where these curves intersect to give steady-state solutions to the 2-cell system. In particular, the partitioning is motivated by the number of roots of Φ and the gradients of F and Φ at the fixed uniform steady state. Specific details of this analysis are given in section A.2 of the appendix, which is preceded by an instructive example for the case when P_a is a constant in section A.1 of the appendix. Here, we illustrate the behavior in each region for particular values of the feedback parameters.

In Figure 7, we display the solution curves of (7) and (11) in the $b_1 - b_2$ plane for specific values of m and n , in each of the twelve regions. Recall that the roots

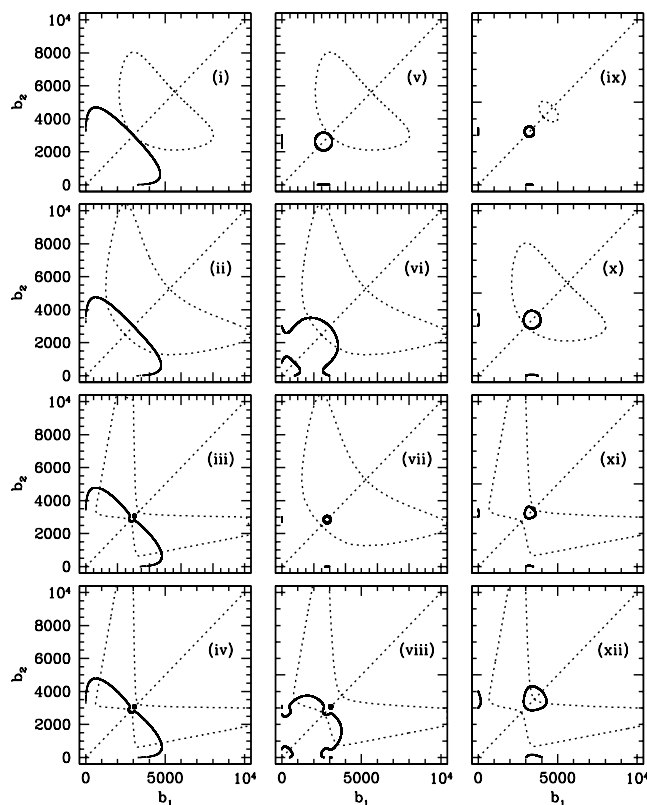


FIG. 7. Illustration of the solutions of (7), $F(b_1) = F(b_2)$ (dashed line), and (11), $\Phi(b_1) = -\Phi(b_2)$ (solid line) for regions (i)–(iv) of the parameter space. Each region is delimited in Figure 6. Uniform solutions of the system are the real roots of Φ , which are the points of intersection of (11) with the line $b_1 = b_2$ in the $b_1 - b_2$ plane. Nonuniform solutions of the system occur if solutions of (11) intersect with the ring of nonuniform solutions to (7). The solution curves of the two equations intersect only for parameters in regions (ii), (iii), (iv), (vi), (viii), (x), and (xii). Therefore, heterogeneous/patterned solutions are possible in these regions. They are also possible in region (xi) for different values of m and n . We note that in region (iv) there are two sets of symmetric heterogeneous solutions (b_1, b_2) : one pair very close to $b_1 = b_2$ and another where b_1 is either much smaller or much larger than b_2 . This may be difficult to see, since the curve intersects the line $b_1 = b_2$ just below $b = \alpha$ and doubles back on itself. The kinetic rate constants are $k_a = 0.0003 \text{ molecule}^{-1} \text{ min}^{-1}$, $k_d = 0.12 \text{ min}^{-1}$, $k_i = 0.019 \text{ min}^{-1}$, $d_a = 0.006 \text{ min}^{-1}$, $d_f = 0.03 \text{ min}^{-1}$. The parameter values C_1 and $C_3 - C_5$ of the production functions are defined through steady-state analysis using $f_{eq} = 3000$, $b_{eq} = 3000$, $r_0 = 3000$, $r_m = 25500$. We fix the parameter $C_2 = 2500$ and vary the Hill coefficients as follows: (i) $m = 0.5$, $n = 3$; (ii) $m = 0.5$, $n = 5$; (iii) $m = 0.5$, $n = 50$; (iv) $m = 0.5$, $n = 65$; (v) $m = 2$, $n = 3$; (vi) $m = 1.5$, $n = 5$; (vii) $m = 2.1$, $n = 5$; (viii) $m = 1.4$, $n = 20$; (ix) $m = 3$, $n = 2.5$; (x) $m = 4$, $n = 3$; (xi) $m = 2$, $n = 30$; (xii) $m = 4$, $n = 30$.

of Φ determine the homogeneous steady states of the full nonlinear system, and that the points of intersection of the solutions to (7) and (11) in the $b_1 - b_2$ plane give the steady states of the 2-cell system. The solutions illustrated in Figure 7 for parameters in regions (i)–(iv) are similar to those in section A.1 of the appendix, in which we assume that P_a is constant. This is to be expected, since the assumption that P_a is constant is equivalent to setting $m = 0$. In the other regions, the number of roots of Φ varies with both m and n , although in our numerical work we have not found more

TABLE 1

In which regions are patterned solutions possible? The partitioning of the parameter space into the twelve regions is illustrated in Figure 6. The solutions are for the particular juxtacrine system demonstrated in Figure 7.

Region of parameter space	Patterned solutions possible?
(i)	no
(ii)	yes
(iii)	yes
(iv)	yes (more than 1)
(v)	no
(vi)	yes
(vii)	no
(viii)	yes
(ix)	no
(x)	yes
(xi)	only for some parameters
(xii)	yes (more than 1 for some parameters)

than four positive real roots. (An explanation for this is given in section A.2 of the appendix.) Consequently, there is some variation in the form of the solution curves of equations (7) and (11), but if these curves do intersect to give patterned solutions to the 2-cell system, then there is generally only one such solution. In Table 1, we list whether each region of the parameter space is capable of 2-cell patterned solutions. The regions where heterogeneous solutions are possible are those satisfying $\Phi(\alpha) > 0$ or $\Phi(\beta) > 0$ (where α and β are the turning points of $F(b)$) and region (iv), in which the ligand feedback parameter $m \leq 1$ and the receptor feedback parameter is very large as well as part of region (xi) adjacent to region (iv).

So far we have considered heterogeneous steady-state solutions to the nonlinear 2-cell model that correspond to a pattern of alternating cell fate in larger arrays. In two dimensions this is equivalent to obtaining alternate stripes of 1-cell width. We have illustrated the existence of such equilibria for a particular juxtacrine mechanism in this section; the details are given in section A.2 of the appendix. However, these results do not give us any information about the stability of the dynamical system. In the next section, we are therefore interested in relating this work to previous results from linear analysis in [21] and also in calculating the stability of the 2-cell solutions obtained above.

5. Comparison with the results of linear analysis. The region of pattern formation where linear analysis predicts that a wavelength of two cells is a possible solution corresponds to part of regions (ii) and (vi), and region (vii), all above the line Σ_2 in Figure 6. As we would expect, in the first two regions we have shown that nonuniform 2-cell patterned equilibria exist. However, in the smaller region (vii) the nonlinear steady-state analysis has demonstrated that there are no 2-cell heterogeneous solutions, contrary to the prediction of the linear system. Note that this significant difference between linear analysis and nonlinear behavior is in contrast to the well-studied Turing systems [12], for which the two behaviors are usually very

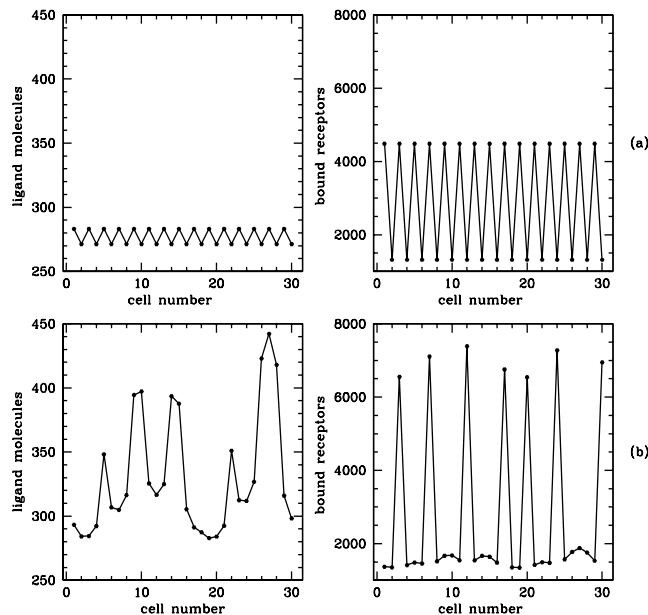


FIG. 8. 2-cell pattern calculated from nonlinear analysis (a) and numerical simulation of the 30-cell system (b) for parameter values in region (ii). The 2-cell system, where alternating cells are identical, is presented on a 30-cell domain for the purposes of comparison. Steady-state analysis of the full system of nonlinear equations has shown that a 2-cell pattern exists for such parameter values, and we observe from numerical simulation of the 2-cell system about the uniform equilibrium (a_{eq}, f_{eq}, b_{eq}) that this solution is stable. When the simulation is carried out on an array of 30 cells, no regular pattern forms, but, more importantly, the pattern wavelength is closer to four cells than two cells. This suggests that although the 2-cell pattern exists as a solution, it is perhaps unstable in larger systems of cells. For brevity, only the profiles of the number of ligand molecules and the number of bound receptors are shown. For the simulation in (b), initial conditions were random perturbations about the homogeneous steady state. The values of the “free” parameters are $m = 0.5$ and $n = 5$. The other parameter values are as in Figure 7.

similar. Numerical simulations on arrays of both 2 and 30 cells for parameters in region (vii) confirm this finding: from initial conditions that are random perturbations about the uniform equilibrium, numerical solutions decay to the trivial homogeneous steady state ($a = b = 0, f = r_0$) in both cases.

There are also regions where 2-cell patterns are solutions of the steady-state equations, but linear analysis does not imply pattern formation. This is to be expected since we have not yet considered the stability of the 2-cell patterns. Moreover, the linear analysis is based only on the behavior of the system close to a single uniform steady state, and when other uniform equilibria exist it is possible that perturbations about these steady states would also give rise to stable patterns for certain parameter values. In Figure 8, we present both the 2-cell pattern calculated from nonlinear analysis, plotted on a 30-cell domain, and a numerical simulation of the 30-cell system for parameters in region (ii). These show that despite the existence of a 2-cell patterned solution and the predictions of linear analysis, longer wavelength patterns are observed in simulations on a larger array of cells. This suggests that for larger systems the 2-cell pattern may be unstable. Such observations raise two important questions: is the 2-cell patterned solution to the steady-state equations stable; and what happens to the stability of this solution in larger systems?

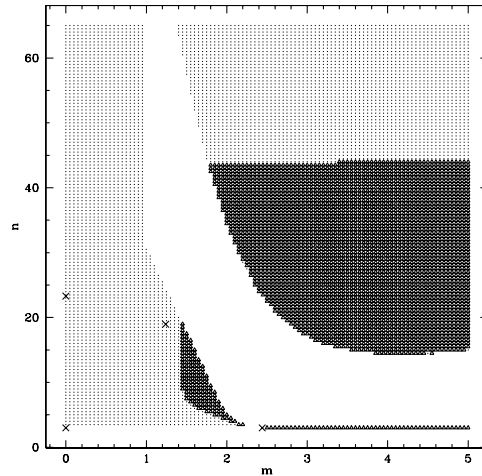


FIG. 9. Stability of the patterned solution to the 2-cell system in $m - n$ parameter space. Light shading indicates stability, and dark shading indicates instability; those regions left blank are where heterogeneous solutions do not exist or they exist for only some parameters (region (xi) of Figure 6). In the case where there are two such solutions (in region (iv) of Figure 6), the stability of the solution where $|b_1 - b_2|$ is the greater is recorded; the other solution is unstable. Note that the pattern is predominantly stable in the region where linear analysis predicts pattern formation; this is the region defined by the four vertices (\times). The other parameter values are as in Figure 7.

5.1. Stability analysis of the 2-cell system. We begin by investigating the stability of the patterned solution for the 2-cell system. The nonuniform equilibria of the 2-cell system can be obtained directly from the steady-state equations of the model, and so it is possible to calculate their stability explicitly. Although algebraically infeasible, we can solve the two nonlinear equations (7) and (9) numerically to find b_1 and b_2 , since we know from section 4 whether (and how many) heterogeneous solutions exist for any point (m, n) of the parameter space outlined in Figure 6. The values of the other variables are obtained by back-substitution into (4) and (8). It is lengthy but straightforward to calculate analytically the Jacobian of the 2-cell system about the nonuniform equilibrium and thus determine the characteristic equation; this is a polynomial of degree six, and a numerical method is used to find the eigenvalues. Figure 9 illustrates the stability of heterogeneous solutions (when they exist) of the 2-cell system in $m - n$ parameter space. We can see that the patterned solution is stable for a range of parameters and is always stable for small m . In the region of pattern formation derived from linear analysis about the uniform steady state, the heterogeneous equilibrium is unstable only close to where there is no solution at all. We therefore conclude that the alternating 2-cell pattern is predominantly stable in the 2-cell regime, and so to try to explain the results of numerical simulations on larger arrays of cells we should now consider its stability in larger systems.

5.2. Investigation of the 1-cell, 2-cell, 4-cell, and 8-cell systems using AUTO. The previous section considered the stability of the patterned solution in the 2-cell system by directly calculating the eigenvalues of the Jacobian. This method could be used to investigate the stability of the 2-cell pattern in larger systems of cells. However, it is more informative to consider all the steady states of the model and their stability for larger arrays of cells, and this is best achieved using AUTO [7], a programming package which can carry out a limited bifurcation analysis of systems

of ODEs.

If we are to track the stability of the 2-cell pattern in larger systems of cells, we need to consider those where a pattern of period 2 cells can exist. It is therefore convenient to study arrays of length 2^i , where i is a positive integer. In this way, we ensure that the 2-cell pattern is always a potential solution and also that as we progress, the equilibria of each system include the equilibria of the previous one. First, we consider the 1-cell system, whose equilibria are the uniform steady states of the full model. We then investigate the 2-cell system, which should include the steady states of the 1-cell system and agree with the stability results of the previous section for the 2-cell pattern. Similarly, in the 4-cell system, we should observe the equilibria of the 2-cell system and so on.

Figure 10 illustrates bifurcation diagrams for a single bound receptor variable in the 1-cell, 2-cell, 4-cell, and 8-cell systems, where one feedback parameter, $m = 0$, is fixed, and the other, n , is free. We confine ourselves to values of n within the region of pattern formation derived from linear analysis to allow comparison with numerical simulations. In the 1-cell case, there is a unique stable steady state for the parameter values shown. If we double the number of cells, then this becomes unstable at a bifurcation point ($n \approx 3$) from which a stable nonuniform steady state branches out. One of the branches gives the equilibrium value of b_1 , while the other gives the corresponding value of b_2 . Taken together, the branches labelled (b) determine a 2-cell patterned solution (b_1, b_2) . In the 4-cell system, the period 2-cell pattern is unstable for small values of n but is stable for n greater than about 6. However, in addition to the 2-cell pattern, there are two other heterogeneous solutions: one of these is stable (labelled (c)) for most of the parameter values, and the other (labelled (d)), which appears just before $n = 6$, is unstable. Both solutions (c) and (d) have only three branches, which means that two of the bound receptor variables have the same value—the smallest value of b . Due to the juxtacrine average, adjacent cells cannot be identical, so, for example, one solution (d) for $n = 10$ would be $b_1 \approx 6400$, $b_2 \approx 1250$, $b_3 \approx 3500$, and $b_4 = b_2$.

Finally, let us consider the behavior of the 8-cell system. We can see by looking at Figure 10 that the bifurcation diagram for 8 cells is much harder to interpret. However, we can observe that the stability of the 2-cell solution remains the same as in the 4-cell system. Furthermore, the stability of the 4-cell pattern labelled (c) in Figure 10 also remains unchanged in the larger system. The most striking feature of the 8-cell diagram is the increase in the number of bifurcations and therefore the number of 8-cell patterns, which illustrates why it becomes difficult to investigate bifurcations in larger systems. This suggests that in large arrays of cells, there are many different patterns of maximum wavelength, but these may be similar to several repetitions of a shorter wavelength. The analysis of the 8-cell system also indicates that a 4-cell pattern exists and is stable for a greater part of the parameter space than the 2-cell pattern on larger domains. This may explain why the alternating 2-cell pattern is observed less frequently than a 4-cell pattern in numerical simulations and also that 2-cell patterns are only stable solutions if n is sufficiently large.

6. Discussion. In this paper, we have considered the behavior of a generic mechanism for juxtacrine signaling in a simple 2-cell system. We have investigated the possibility of heterogeneous solutions, which correspond to a pattern of alternating cell fate in larger systems, and we have obtained conditions on the feedback functions that are sufficient for their existence in general and necessary for their existence in a specific case. Furthermore, we have calculated the stability of the patterned

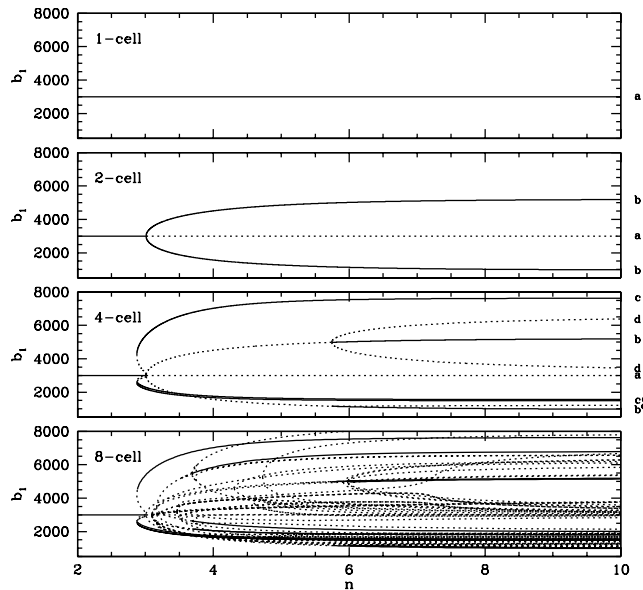


FIG. 10. Bifurcation diagrams for the variable b_1 in the 1-cell, 2-cell, 4-cell, and 8-cell systems, where the receptor feedback parameter n is free. Solid lines denote stable equilibria, and dotted lines denote unstable equilibria. The solution of the 1-cell system gives the uniform equilibria of the full model. Although we plot only a single bound receptor variable against n , these diagrams are in fact the same for all b_j , since the boundary conditions are periodic. In this way, a solution of the system of cells is comprised of one or more paths on the diagram; each solution is labelled by a single letter. For example, in the 2-cell case, the stable solution (b) that branches away from $b_1 = 3000$ in two directions represents the heterogeneous steady state derived in section 4. In the case of 4 cells, the solutions of both the 1-cell and 2-cell systems remain in addition to one stable (c) and one unstable (d) 4-cell pattern. The important observation is that in the 4-cell system there is a 4-cell pattern which is stable for most values of n , whereas the 2-cell pattern is stable only for $n > 6$. Furthermore, even though the 8-cell diagram is difficult to interpret, we can check that the stability of the period 2-cell and 4-cell patterns is the same as in the 4-cell system. The ligand feedback parameter $m = 0$. The other parameter values are as in Figure 7.

equilibria in the 2-cell domain and compared these results with previous work, which applied linear analysis techniques to the full model. In addition, we have conducted a bifurcation analysis of 1-cell, 2-cell, 4-cell, and 8-cell arrays to address the behavior of the model in larger systems of cells. Our results confirm numerical evidence that juxtacrine signaling, with positive feedback in ligand and receptor production, can generate a wide range of stable spatial patterns. Note that this runs counter to recent thinking in developmental biology that such “lateral induction” will prevent patterning (e.g., [10]).

We have shown that a pattern of wavelength two cells exists as a steady-state solution to the juxtacrine model (1) in a significant part of parameter space. Moreover, when there is a single homogeneous steady state, this pattern is always stable on a domain of two cells. It is not surprising that this is predominantly true for parameters for which the linear analysis of [21] predicts that a pattern of wavelength two is an unstable mode. However, stable 2-cell patterns do exist outside the region of pattern formation derived from our linear analysis, and, more importantly, numerical simulations on large arrays of cells show that patterns do form for these parameters. Furthermore, for a small part of the region of pattern formation derived from our

linear analysis, we have shown that no patterned equilibria exist in the 2-cell system; likewise, in numerical simulations on large domains, no patterned solutions are generated. These two observations highlight a distinct difference between the linear analysis and nonlinear behavior. They suggest that knowing when patterns form in the nonlinear 2-cell model is more informative for an understanding of the behavior in larger systems than considering the linearized model for larger arrays of cells. This is quite different from diffusion-driven patterns in reaction-diffusion or Turing systems, in which the results of linear analysis typically give a very good understanding of the behavior of the full model [12]. It is worth noting that the model we study cannot be thought of as a discrete analogue to these continuous systems: the nature of the spatial coupling distinguishes the juxtacrine mechanism from any discretized version of reaction-diffusion models. However, the methods employed by authors investigating spatial patterns [3, 17] and waves [22] in discrete Laplacian systems might be applicable to our model; this is an area for future work.

Investigation of the 2-cell system does not explain why regular 2-cell patterns are not generated in numerical simulations on large arrays of cells. To understand such behavior we must turn to the results of the bifurcation analysis. There are two main conclusions to be drawn from this work. First, the number of stable patterned solutions increases as both the strength of receptor feedback increases and the size of the system/domain increases. Second, the 2-cell pattern is not seen numerically for weaker feedback in receptor production because it becomes unstable in larger systems, although it remains stable if the feedback is strong enough. This leads us to speculate that the pattern we expect to dominate in large systems of cells corresponds most closely to the shortest stable wavelength for any given parameter values.

Previously, pattern formation in juxtacrine models has been considered only in the mechanism proposed by Collier et al. [6]. The assumption of negative feedback in ligand production in their model gives rise only to patterns of alternate cell fate. The positive feedback we have assumed is well established for a ligand molecule called transforming growth factor- α that binds to a receptor called epidermal growth factor receptor [4, 5]. This is a mechanism for which there is a comprehensive amount of kinetic data and as such is the reference for the values of our fixed parameters [20]. However, there is recent evidence that, in some contexts, the biological system modelled by Collier et al.—Delta-Notch [1, 8, 10, 16]—and many other signaling molecules [18] are also subject to such positive feedback. In particular, it is thought that the production of both new ligands and new receptors is upregulated via binding during wing morphogenesis of the fruitfly [2]. In this process, sharp bands of receptor (Notch) expression develop at the vein-intervein boundaries.

Collier et al. also investigated their model on a domain of just two cells, although the results of their linear analysis agreed well with numerical studies. An important difference between the behavior of the 2-cell system of their mechanism and that studied in this paper is highlighted by an interpretation of the possible patterns on a two-dimensional square grid. In the Collier et al. model, their assumption of the juxtacrine average corresponds to checks/spots in two dimensions, whereas our average corresponds to stripes. Two-dimensional numerical simulations of the model (1) on large arrays of cells have been conducted [15], and we do see a variety of spotted and striped patterns, although the spots are in general a few cell lengths apart. Collier et al. also presented simulations on two-dimensional hexagonal arrays, but these did not give rise to striped patterns. The principal differences between their model and ours are in the feedback assumptions and the representation of juxtacrine signaling. From

a biological point of view, it would be interesting to know whether the formation of stripes is in fact a consequence of our assumption of positive feedback in ligand and receptor production. This forms a basis for further investigation of our model with different juxtacrine averages and negative feedback.

In summary, we can conclude that a 2-cell pattern of alternating cell fate exists as a steady-state solution to the full nonlinear model. However, the stability of this solution changes as the domain size increases, and in larger systems the 2-cell pattern is stable only for large enough feedback in receptor production. In applications, we are concerned with pattern formation on domains of tens or hundreds of cells, and to address this, we refer back to Figure 3. In this figure, we present three numerical simulations of the model on a 30-cell domain for a particular set of parameter values but each with different (random) initial conditions. For these parameter values, the linear analysis predicts that the only unstable mode is one of wavelength two cells. Our nonlinear analysis shows that a nonlinear pattern of wavelength two cells exists and is stable on a domain of two cells. However, our numerical bifurcation study demonstrates that the 2-cell pattern is unstable on a larger domain (even on a domain of four cells) but that a 4-cell pattern is stable on larger domains.

In fact, the patterns presented in Figure 3 are of wavelength 30, since there is no regular repetition of one wavelength. However, the pattern is approximately of wavelength 4 with some irregularities. Figure 3 illustrates three patterns of this form, and in fact numerical simulations reveal many different patterns, all of wavelength 30 but approximately of wavelength 4. We speculate that as the domain size increases, the bifurcation diagram for patterns becomes extremely complex (recall the case of 8 cells in Figure 10), giving rise to many patterns of the same basic structure but with minor differences in detail. In reality, the fine-grained patterns that one sees in early development typically have approximate periodicity but with some irregularities. Our work predicts that this is not due to environmental heterogeneity; rather, it is an intrinsic feature of the patterning dynamics.

Appendix. In section 3, we discussed our approach to finding patterned solutions to the 2-cell system. We then outlined in section 4 the necessary conditions for this type of solution when the production functions are of Hill form. In this appendix we provide the details of that work. In addition to presenting the analysis behind the specific case described in section 4, we first illustrate the process for a simpler example. However, before doing so we need to determine the condition for solutions $b_1 \neq b_2$ to (7) when P_f is of Hill form:

$$P_f(b) = C_3 + \frac{C_4^m b^n}{C_5^n + b^n},$$

where C_3, C_4, C_5 are positive constants and n is some real number greater than zero. Recall (from section 3) that for such a solution, $F'(b) = 0$ (where $F(b) = b/P_f(b)$), which now becomes

$$C_3 + \frac{C_4^n b^n}{C_5^n + b^n} - \frac{n C_4^n C_5^n b^n}{(C_5^n + b^n)^2} = 0,$$

must have a real and positive solution. After some rearranging, this equation is just a quadratic in b^n which may be solved to obtain

$$(A.1) \quad b^n = \frac{C_5^n \{(n-1)C_4^n - 2C_3 \pm \sqrt{(n-1)^2 C_4^{2n} - 4n C_3 C_4^n}\}}{2(C_3 + C_4^n)}.$$

Thus for real $b > 0$, there are at most two possible stationary points of F , and these exist if the following inequality holds:

$$(A.2) \quad (n-1)^2 C_4^m > 4n C_3.$$

It is straightforward to show that if two stationary points of F exist, they are also turning points. For fixed C_3 and C_4 , we therefore have a condition on n which determines whether nonuniform solutions of (7) exist. Figure 4a plots F for an n satisfying the above inequality. The corresponding solutions of (7) in the $b_1 - b_2$ plane are illustrated in Figure 4b.

A.1. Illustrative example: P_a is a constant. In this section, we represent solutions of (11) in the $b_1 - b_2$ plane for two particular forms of the function Φ and demonstrate how these can intersect with the solutions of $F(b_1) = F(b_2)$. Specifically, we consider the simple case when P_a is just a constant and therefore $H = P_a - k_i b$ is a straight line with negative slope. We assume that P_f is such that $1/G = b/(P_f - k_i b)$ is a positive function for $b > 0$ with two turning points, α and β , (these are defined by (A.1) if P_f is of Hill form). Furthermore, we assume that the function $1/G$ has a unique point of inflection between α and β .

Recall that the roots of Φ are the points of intersection of H and c/G , where c is a positive constant defined in section 3. The gradient of c/G is equal to $-k_i$, the gradient of H , at a maximum of two points: the gradient of c/G is negative only for $b \in (\alpha, \beta)$, and between α and β there is only a single point of inflection. Consequently, H and c/G have a maximum of three points of intersection. This is equivalent to saying that Φ has at most three real roots, and so we consider the following two cases separately: (I) Φ has a single real root, and (II) Φ has three real roots. The case when Φ has two real roots is just the point of transition between (I) and (II). Figure 11 shows qualitative forms for Φ in each case, as well as the corresponding solutions of $\Phi(b_1) = -\Phi(b_2)$ in the $b_1 - b_2$ plane. Since the equation is symmetric, we need only consider $b_1 < b_2$ and reflect the solution in the line $b_1 = b_2$.

Case (I). The function Φ is strictly decreasing with a single real root, say, $b = b_{eq}$. Therefore, for $b_1 < b_{eq}$ there is a unique value of b_2 satisfying (11). This leads to a single curve of solutions in the $b_1 - b_2$ plane, symmetric about the line $b_1 = b_2$ (illustrated in Figure 11).

Case (II). Φ has three real roots, so it is convenient to consider the values of b_1 in successive intervals. We denote the roots of Φ by $b_{e1} < b_{eq} < b_{e2}$, and we define $\tilde{b}_{e1} < b_{e1}$ and $\tilde{b}_{e2} > b_{e2}$ such that $\Phi(\tilde{b}_{e1}) = -\Phi_{min}$ and $\Phi(\tilde{b}_{e2}) = -\Phi_{max}$, where Φ_{min} and Φ_{max} are the values of Φ at its minimum and maximum turning points, respectively (illustrated in Figure 11). We then tabulate the solutions b_2 in Table 2. As shown in Figure 11, case (II) gives both a curve and a ring of solutions in the $b_1 - b_2$ plane. The difference in the magnitudes of Φ_{min} and Φ_{max} determines the size of the closed loop and where it intersects the line $b_1 = b_2$. Figure 11 illustrates solutions for $|\Phi_{min}| > |\Phi_{max}|$.

Now that we have constructed solutions to $\Phi(b_1) = -\Phi(b_2)$ in the $b_1 - b_2$ plane, we can consider conditions that guarantee an intersection with the solution curve of $F(b_1) = F(b_2)$, thus giving a nonuniform solution to the 2-cell system. For case (I), this occurs if the root of Φ lies between the turning points of the function F (these are just the turning points of $1/G$), which implies that $F'(b_{eq}) < 0$. From (10) it then follows that

$$(A.3) \quad P'_f(b_{eq}) > \frac{P_f(b_{eq})}{b_{eq}},$$

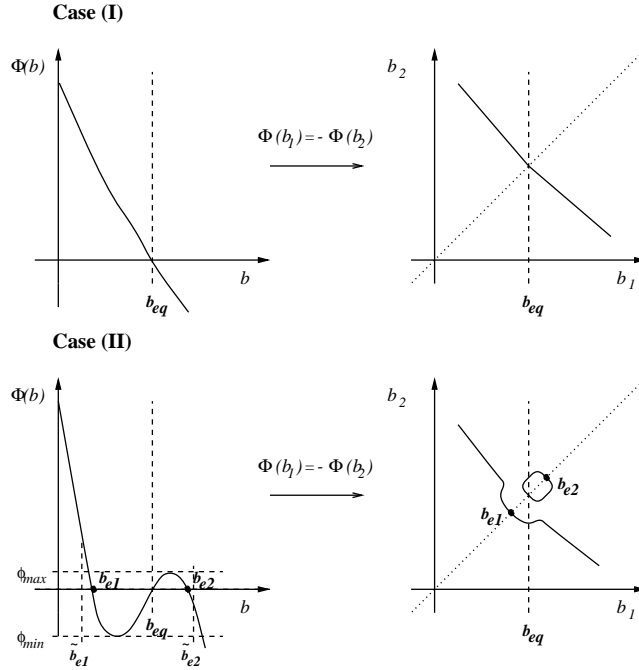


FIG. 11. Qualitative illustration of $\Phi(b)$ and solutions of $\Phi(b_1) = -\Phi(b_2)$ in the $b_1 - b_2$ plane for the simple example: P_a is a constant. We consider the cases when Φ has either a single real root (I) or three real roots (II). Since P_a is a positive constant, $\Phi(0) > 0$. In (I), Φ is strictly decreasing, crossing the b -axis at $b = b_{eq}$. Thus for $b_1 < b_{eq}$ there is a unique value of b_2 satisfying (11), corresponding to a single curve of solutions in the $b_1 - b_2$ plane, symmetric about the line $b_1 = b_2$. Case (II) is more complicated since Φ changes sign three times. This results in both a curve and a detached ring in the $b_1 - b_2$ plane. The ring occurs when the magnitude of Φ differs at the two turning points. In this figure we have assumed that $|\Phi_{min}| > |\Phi_{max}|$, so that the curve passes through the smallest root. If this condition was reversed, then the curve would intersect the largest root, and the loop would form between the smaller roots instead.

giving us a sufficient condition for a heterogeneous solution when Φ has only one root. We have considered a general form of P_f for which heterogeneous solutions to (7) exist. Since the specific shape of these solutions in the $b_1 - b_2$ plane (see, for example, Figure 4) depends on the details of P_f , we therefore cannot dismiss the possibility of intersections with solutions to (7) below α and above β . As such, the inequality (A.3) is not a necessary condition for patterned solutions in this illustrative example. However, in section A.2 we shall show that this is a necessary condition when P_a is a constant for a particular juxtacrine system.

In case (II), when Φ has three real roots, at least one of them must lie between α and β (the turning points of F and $1/G$). For the purposes of illustration, we therefore assume that $b = b_{eq}$ is always an equilibrium in the interval (α, β) . Since $\Phi'(b_{eq}) < 0$ when $b = b_{eq}$ is a unique root, three steady states of which b_{eq} is the middle root exist for $\Phi'(b_{eq}) > 0$. We note that three steady states can of course exist for $\Phi'(b_{eq}) < 0$, so that b_{eq} is either the smallest or largest root, and a similar analysis to that below can be done. We are now interested in where the other roots of Φ lie along the line $b_1 = b_2$ in relation to α and β , which is determined by considering the sign of $\Phi(\alpha)$ and $\Phi(\beta)$. For example, if $\beta < b_{e1}$, then $\Phi(\beta) > 0$, and if $\alpha > b_{e2}$, then $\Phi(\alpha) < 0$. For the form illustrated in Figure 11, where $|\Phi_{min}| > |\Phi_{max}|$ so that the curve intersects

TABLE 2

Case (II): $\Phi(b)$ has three real roots. The number of solutions b_2 that satisfy $\Phi(b_1) = -\Phi(b_2)$, where b_1 is in a particular interval. *For $b_1 \in (b_{e1}, b_{eq})$, if the magnitude of Φ is greater at the maximum turning point than at the minimum turning point, there are two solutions $b_2 \in (b_{eq}, b_{e2})$. If the reverse is true, then there will be some values of b_1 in this interval for which there is no solution b_2 .

Interval of b_1	Number of solutions b_2
$[0, \tilde{b}_{e1})$	1
\tilde{b}_{e1}	2
(\tilde{b}_{e1}, b_{e1})	3
b_{e1}	2
(b_{e1}, b_{eq})	2 {or 0 for some b_1 if $ \Phi_{min} > \Phi_{max} $ }*
$[b_{eq}, b_{e2})$	1

TABLE 3

Case (II): $\Phi(b)$ has three real roots, and $|\Phi_{min}| > |\Phi_{max}|$. The number of patterned solutions (i.e., solutions satisfying both $\Phi(b_1) = -\Phi(b_2)$ and $F(b_1) = F(b_2)$ with $b_1 \neq b_2$) for each of the possible configurations that are illustrated in Figure 12. The sign of $\Phi(\alpha)$ (or $\Phi(\beta)$) determines the size of α (or β) in relation to the smallest (or largest) root of Φ .

	$\Phi(\alpha)$	$\Phi(\beta)$	Number of patterned solutions
(a)	+ve	+ve	2 pairs (b_1, b_2)
(b)	+ve	-ve	1 pair (b_1, b_2)
(c)	-ve	+ve	1 or 3 pairs (b_1, b_2)
(d)	-ve	-ve	0 or 2 pairs (b_1, b_2)

the smallest root and a closed loop joins the other roots, the existence of solutions can then be summarised in Table 3. These four configurations are displayed in Figure 12. Notice that more than one symmetric pair of nonuniform solutions are possible in case (II), since both the curve and ring of solutions to (11) can intersect with the solutions of (7). Moreover, in configurations (c) and (d), the open curve of solutions to (11) can intersect twice with the heterogeneous solutions of (7), and thus up to three pairs of nonuniform solutions are possible.

In summary, for this illustrative example when the production function P_a is a constant, we have considered the two possible forms of Φ and derived conditions for patterned solutions in each case. If Φ has a single real root, say, b_{eq} , then patterned solutions always exist if $F'(b_{eq}) < 0$, i.e., if b_{eq} lies between α and β —the turning points of F . In the case of three real roots, patterned solutions always exist if $\Phi(\alpha)$ and $\Phi(\beta)$ are of different sign, so that only one or all roots of Φ lie between the turning points of F . These are all sufficient conditions; other possibilities are dependent on the details of P_f . However, we recall that for any patterned solutions to exist, it is necessary that $F'(b) = 0$ for some $b > 0$. In the following section, we consider the production functions P_a and P_f to be of Hill form for a particular parameter system. Provided that the positive constant k_i is sufficiently small, the assumptions made about P_f in this section are satisfied by the Hill function form.

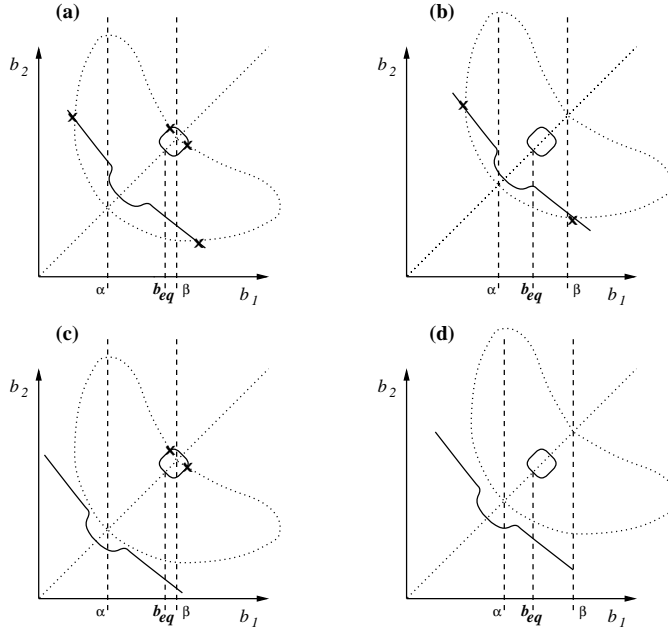


FIG. 12. Qualitative solutions of $\Phi(b_1) = -\Phi(b_2)$ (solid lines) and $F(b_1) = F(b_2)$ (dotted lines) in the $b_1 - b_2$ plane for case (II) of the simple example: P_a is a constant. Each diagram corresponds to one of the configurations listed in Table 3. The points of intersection of the two sets of solutions (\times) represent the nonuniform solutions of the full 2-cell system. As in Figure 11, we have assumed that $|\Phi_{min}| > |\Phi_{max}|$. Notice that configurations (c) and (d) can give two additional pairs of heterogeneous solutions to those demonstrated above; if the smallest root of Φ , b_{e1} , is sufficiently close to α yet still smaller than α , then the solid curve which passes through b_{e1} will intersect twice with the dotted curve of nonuniform solutions to $F(b_1) = F(b_2)$.

A.2. Partitioning of the parameter space when P_a and P_f are of Hill function form. We now give details of how we partitioned the parameter space into the twelve regions shown in Figure 6. The behavior in each region is demonstrated for particular values of the feedback parameters m and n in Figure 7 of the main text. The analysis that follows is a study for a particular system in which all but two parameters are fixed. Although the framework is quite general, any conditions that are derived for patterned solutions are specific to this system.

We recall that solutions of the full 2-cell system must satisfy both (7) and (11). The first of these equations depends on only one of the production functions, P_f , and, as discussed at the beginning of this appendix, for patterned equilibria to exist, the equation $P_f(b) - bP'_f(b) = 0$ must have at least one positive real root. For P_f of Hill form, we obtained a condition (A.2) on the function parameters C_4 , C_5 , and n such that (10) has two positive real roots. Since we determine all parameters except n by steady-state analysis, this now corresponds to a condition on n . We denote the critical value of n by n_{crit} and the line $n = n_{crit}$ by Σ_1 , which gives us our first condition in $m - n$ parameter space: for values of n below Σ_1 nonuniform solutions are not possible. As n increases above the line Σ_1 , the function F remains qualitatively the same, so we now concentrate on the form of Φ and investigate where the solutions of (7) and (11) intersect.

The function $\Phi = H - c/G$, which depends on both production functions, is more complicated than in section A.1 since P_a now depends on b . Indeed, the function H

can have up to two nonzero real roots for $m > 0$, since $P_a(b)$ intersects the straight line $k_i b$ at $b = 0$ and at one or two other points. The exact number of roots depends on whether P_a has a point of inflection (recall that for all $b > 0$, $P_a(b)$ is a positive, increasing function): if $P_a''(b) < 0$ for all $b > 0$ then P_a can intersect $k_i b$ at only one nonzero point, but if there is a value of $b > 0$ for which $P_a''(b) = 0$, then there can be a further point of intersection. Since P_a is of Hill form, it has a unique point of inflection for $m > 1$. Thus the change in the number of roots occurs at $m = 1$, so that for $m \leq 1$, H has one nonzero real root, whereas for $m > 1$, H has two nonzero real roots. This in turn increases the number of roots of Φ . In Figure 6 we denote the line $m = 1$ by Σ_5 .

Regions (i)–(iv). Let us begin by considering $m \leq 1$, the region to the left of Σ_5 in $m - n$ parameter space. This can be subdivided into regions (i)–(iv) by the conditions $\Sigma_2 - \Sigma_4$, as demonstrated in Figure 6. In each of these regions, Φ has different properties. The fixed nonzero real root b_{eq} is the only root in region (i) and in most of region (ii). The line Σ_2 denotes $F'(b_{eq}) = 0$, so that above Σ_2 , $F'(b_{eq}) < 0$, and therefore $\alpha < b_{eq} < \beta$; recall that α and β are the roots of $F' = 0$. Below Σ_2 , $b_{eq} < \alpha$ or $b_{eq} > \beta$, depending on whether $C_5^n(n-1)/(n+1) - b_{eq}^n$ is positive or negative, respectively. For the parameter values of the juxtacrine mechanism we use, $b_{eq} < \alpha$ below Σ_2 . We note that the line Σ_2 is identical to the line \mathcal{L}_4 of Figure 2 derived in our linear analysis. In regions (iii) and (iv) of Figure 6, Φ has at least three nonzero real roots: extra roots occur as the slope of Φ at $b = b_{eq}$ changes sign. This is represented in $m - n$ parameter space by the line $\Phi'(b_{eq}) = 0$, denoted by Σ_3 . The line Σ_3 is the line \mathcal{L}_1 of Figure 2 derived in our linear analysis. Above Σ_3 , $\Phi'(b_{eq}) > 0$, and b_{eq} becomes the second of three nonzero real roots. Just below Σ_3 , there is also a transition between one, two, and three real roots for which b_{eq} is either the smallest or largest root. (For our fixed parameter values it is the largest root.) Therefore, in region (ii), b_{eq} is not the only root close to the line Σ_3 ; although obtaining an expression as to when this transition occurs is difficult because we cannot solve $\Phi(b) = 0$ or $\Phi'(b) = 0$ explicitly. However, this does not affect the possibility of patterned solutions in region (ii).

For the particular system we look at, we observe only three positive real roots in regions (iii) and (iv), although we cannot rule out that there are further roots for other fixed parameter values. This is because P_f is of Hill function form, so that, unlike in section A.1, the function $1/G$ can have more than one point of inflection between its turning points, α and β . We distinguish between regions (iii) and (iv) by looking at the sign of $\Phi(\alpha)$, since this affects where solution curves of (11) intersect with those of (7). From numerical calculations, $\Phi(\alpha)$ is positive for values of m and n between the line Σ_2 and the curve Σ_4 and negative elsewhere. Thus, in region (iii), $\Phi(\alpha) > 0$, whereas in region (iv), $\Phi(\alpha) < 0$.

The four left-hand plots of Figure 7 show the solution curves of (7) and (11) in the $b_1 - b_2$ plane for parameter values in each of the regions (i)–(iv). As expected, these graphs are similar to those illustrated in section A.1, where we assumed P_a was a constant, which is equivalent to $m = 0$. We see that nonuniform solutions are not possible in region (i) and that condition (A.3) derived in case (I) of section A.1 must hold for $m \leq 1$. Solutions in regions (iii) and (iv), where Φ has three nonzero real roots, correspond to configurations (b) and (d) of Figure 12, respectively. The other configurations are not seen because $\Phi(\beta)$ is not positive for $m \leq 1$. We note that $\Phi(\beta)$ is only positive in region (xii), which will be discussed later.

Regions (v)–(viii). We now address what happens for $m > 1$. This implies that the function H has two positive real roots, and consequently Φ has at least two positive real roots. In regions (v) and (vii), Φ has only two such roots with b_{eq} the larger. This is also true for most of region (vi): another two roots exist close to Σ_3 , as explained above for region (ii), but this does not affect the possibility of patterned solutions. Below the line Σ_2 , in region (v), both roots of Φ are smaller than α since $b_{eq} < \alpha$. In regions (vi) and (vii), $\alpha < b_{eq} < \beta$. However, in region (vi), $\Phi(\alpha) > 0$, and therefore α lies between the two roots, whereas in region (vii), $\Phi(\alpha) < 0$ and so α is smaller than both roots. This is demonstrated in Figure 7 for specific values of m and n . We remark that when $|\Phi_{min}| > |\Phi_{max}|$, the solutions of (11) are closed loops joining the two homogeneous equilibria. When the inequality is reversed, the solutions form two open curves, each intersecting a single homogeneous steady state. Note that only parameters in one of these regions, region (vi), are capable of producing heterogeneous solutions.

For parameter values in region (viii), Φ has at least four nonzero real roots, since another two roots exist for $\Phi'(b_{eq}) > 0$. As mentioned above, parameter values above the line Σ_3 in $m - n$ parameter space satisfy this condition. However, the solutions of $\Phi(b_1) = -\Phi(b_2)$ in the $b_1 - b_2$ plane for region (viii) are still quite similar to those of region (vi). In Figure 7 we can see that both (vi) and (viii) have two curves of solutions to (11). In addition, (viii) has a small ring of solutions, but this does not result in further intersections with solutions of (7), and therefore parameters in both of these regions give one symmetric set of heterogeneous solutions (b_1, b_2) .

Regions (ix)–(xii). The right-hand plots of Figure 7 show the solutions of (7) and (11) for parameters in the final four regions: (ix)–(xii). In regions (ix) and (x), Φ has only two nonzero real roots, where $b_{eq} < \alpha$ is the smaller. The difference between the two regions is that in (ix), $\Phi(\alpha)$ is negative so that both roots lie below α , whereas in (x), $\Phi(\alpha)$ is positive so that the larger root must lie above α . Thus, as Figure 7 demonstrates, no nonuniform solutions exist for parameters in region (ix), but they must exist for those in region (x).

We have not fully investigated the regions denoted by (xi) and (xii). From numerical observations of our particular system, we see that Φ has two nonzero real roots for most parameters in both regions; Φ seems to have four nonzero real roots for values of n above region (viii). If Φ has only two real roots (the case illustrated in Figure 7), then b_{eq} must be the smaller of the two roots, since both regions lie above Σ_3 , and therefore $\Phi'(b_{eq}) > 0$. However, Φ may still develop more than two turning points. This leads us to believe that there are nonzero roots smaller than b_{eq} , but that these have become complex in regions (xi) and (xii). The important difference is that in region (xii), β lies between the two roots so that the curves of (7) and (11) must intersect to give nonuniform solutions, which does not occur for parameter values in region (xi). For those values in region (xi) where Φ has four nonzero real roots, the solution curves are similar to those shown in Figure 7 of region (viii), except that $\Phi(\alpha) < 0$, so there are possibly two sets of heterogeneous solutions. Similarly, if Φ has four nonzero real roots in region (xii), then there are possibly three sets of patterned solutions since $\Phi(\beta) > 0$. Therefore, patterned solutions are possible for all parameters in region (xii), but this is not true for all parameters in region (xi).

Limit on the number of roots of Φ . Numerical investigation of the parameter space for our particular juxtacrine system leads us to conclude that, for the fixed parameter values we use, there are at most four positive real roots of Φ . Analysis of the function Φ shows that this is not a general property, even when P_a and P_f

are restricted to Hill function form, and that for suitable parameters we could obtain more roots and therefore more complicated solutions to $\Phi(b_1) = -\Phi(b_2)$ in regions above the line denoted by Σ_3 in Figure 6. However, the nature of juxtacrine signaling allows us to make a simplifying assumption. The rate of internalization of bound receptors, k_i , is small in juxtacrine communication because the process of internalizing the ligand-receptor complex is difficult: the ligand must become detached from the neighboring cell's membrane. We can thus obtain a good approximation to the system by considering $k_i = 0$. On making this substitution in (12), Φ then becomes

$$\Phi^*(b) = P_a(b) - c^*F(b),$$

where $c^* = d_a d_f k_d / k_a$ and $F(b) = b / P_f(b)$, as defined at the beginning of this section. The roots of Φ^* are just the points of intersection of P_a and $c^*F(b)$. We know that P_a is a monotonically increasing function of b with a single point of inflection for $m > 1$ at

$$b = C_2 \left(\frac{m-1}{m+1} \right)^{\frac{1}{m}}.$$

The function $F(b)$ is strictly positive for $b > 0$ and has two turning points $\alpha < \beta$ defined by (A.1). For P_f of Hill function form and $b > 0$, $F(b)$ has only a single point of inflection which lies in the interval (α, β) , and this ensures that there are at most four nonzero real roots, say, $b_a < b_b < b_c < b_d$, such that $b_a < b_b < \alpha$, $\alpha < b_c < \beta$, and $b_d > \beta$, as well as the trivial root $b = 0$. We therefore expect the full system to behave in a similar way for the biologically relevant case of small k_i . As an aside, we remark that the line Σ_7 in Figure 6 denotes the equality $H'(b_{eq}) = P'_a(b_{eq}) - k_i = 0$, so that for $m < \Sigma_7$, $H'(b_{eq}) < 0$. If we were to set $k_i = 0$, then $H'(b_{eq}) > 0$ for all $m > 0, n > 0$, and so the parameter space would consist only of those regions where m lies to the right of the line Σ_7 in Figure 6.

Acknowledgment. We thank Markus Owen for helpful discussions.

REFERENCES

- [1] J. F. DE CELIS AND S. BRAY, *Feedback mechanisms affecting notch activation at the dorsoventral boundary in the Drosophila wing*, Development, 124 (1997), pp. 3241–3251.
- [2] J. F. DE CELIS, S. BRAY, AND A. GARCIA-BELLIDO, *Notch signalling regulates veinlet expression and establishes boundaries between veins and interveins in the Drosophila wing*, Development, 124 (1997), pp. 1919–1928.
- [3] S.-N. CHOW, J. MALLET-PARET, AND E. S. VAN VLECK, *Pattern formation and spatial chaos in spatially discrete evolution equations*, Random Comput. Dynam., 4 (1996), pp. 109–178.
- [4] A. J. L. CLARK, S. ISHII, N. RICHERT, G. T. MERLINO, AND I. PASTAN, *Epidermal growth factor regulates the expression of its own receptor*, Proc. Natl. Acad. Sci. USA, 82 (1985), pp. 8374–8378.
- [5] R. J. COFFEY, R. DERYNCK, J. N. WILCOX, T. S. BRINGMAN, A. S. GOUSTIN, H. L. MOSES, AND M. R. PITTELKOW, *Production and auto-induction of transforming growth factor- α in human keratinocytes*, Nature, 328 (1987), pp. 817–820.
- [6] J. R. COLLIER, N. A. M. MONK, P. K. MAINI, AND J. H. LEWIS, *Pattern formation by lateral inhibition with feedback: A mathematical model of Delta-Notch intercellular signalling*, J. Theoret. Biol., 183 (1996), pp. 429–446.
- [7] E. J. DOEDEL, H. B. KELLER, AND J. P. KERNÉVEZ, *Numerical analysis and control of bifurcation problems: (I) Bifurcation in finite dimensions*, Internat. J. Bifur. Chaos Appl. Sci. Engrg., 1 (1991), pp. 493–520.
- [8] S. S. HUPPERT, T. L. JACOBSON, AND M. A. T. MUSKAVITCH, *Feedback regulation is central to Delta-Notch signalling required for Drosophila wing vein morphogenesis*, Development, 124 (1997), pp. 3283–3291.

- [9] J. LEWIS, *Neurogenic genes and vertebrate neurogenesis*, Curr. Op. Neurobiol., 6 (1996), pp. 3–10.
- [10] J. LEWIS, *Notch signalling and the control of cell fate choices in vertebrates*, Sem. Cell Dev. Biol., 9 (1998), pp. 583–589.
- [11] J. MASSAGUÉ, *Transforming growth factor- α : A model for membrane-anchored growth factors*, J. Biol. Chem., 265 (1990), pp. 21393–21396.
- [12] J. D. MURRAY, *Mathematical Biology*, 2nd ed., Springer-Verlag, Berlin, 1993.
- [13] M. A. T. MUSKAVITCH, *Delta-Notch signalling and Drosophila cell fate choice*, Dev. Biol., 166 (1994), pp. 415–430.
- [14] M. R. OWEN AND J. A. SHERRATT, *Mathematical modelling of juxtacrine cell signalling*, Math. Biosci., 152 (1998), pp. 125–150.
- [15] M. R. OWEN, J. A. SHERRATT, AND H. J. WEARING, *Lateral induction by juxtacrine signalling is a new mechanism for pattern formation*, Dev. Biol., 217 (2000), pp. 54–61.
- [16] V. M. PANIN, V. PAPAYANNOPOULOS, R. WILSON, AND K. D. IRVINE, *Fringe modulates Notch-ligand interactions*, Nature, 387 (1997), pp. 908–912.
- [17] E. PLAhte, *Pattern Formation in Discrete Cellular Lattices with Internal Cell Dynamics and Regulated Cell-Cell Interaction*, preprint, Department of Mathematical Sciences, Agricultural University of Norway, Aas, Norway, 1999.
- [18] K. M. REILLY AND D. A. MELTON, *Short-range signaling by candidate morphogens of the TGF beta family and evidence for a relay mechanism of induction*, Cell, 86 (1996), pp. 743–754.
- [19] A. M. TURING, *The chemical basis of morphogenesis*, Phil. Trans. R. Soc., B237 (1952), pp. 37–72.
- [20] C. M. WATERS, K. C. OBERG, G. CARPENTER, AND K. A. OVERHOLSER, *Rate constants for binding, dissociation, and internalization of EGF: Effect of receptor occupancy and ligand concentration*, Biochem., 29 (1990), pp. 3563–3569.
- [21] H. J. WEARING, M. R. OWEN, AND J. A. SHERRATT, *Mathematical modelling of juxtacrine patterning*, Bull. Math. Biol., 62 (2000), pp. 293–320.
- [22] B. ZINNER, G. HARRIS, AND W. HUDSON, *Traveling wavefronts for the discrete Fisher's equation*, J. Differential Equations, 105 (1993), pp. 46–62.